CORA Cork Open Research Archive
Cartlann Taighde Oscailte Chorcaí

Title	Co-designed quasi-reflectionless low-noise amplifier with bandpass filter and RF switching functionalities
Authors	Cheng, Steven Matthew;Fontana, Andres;Psychogiou, Dimitra
Publication date	2026-04-01
Original Citation	Cheng, S M, Fontana, A & Psychogiou, D 2026, 'Co-designed quasi-reflectionless low-noise amplifier with bandpass filter and RF switching functionalities', IEEE Microwave and Wireless Technology Letters, vol. 36, no. 9, pp. 1490-1493. https://doi.org/10.1109/LMWT.2026.3676313
Type of publication	Article (peer-reviewed)
Link to publisher's version	https://www.webofscience.com/api/gateway?GWVersion=2&SrcApp=pureucc&SrcAuth=WosAPI&KeyUT=WOS:001732790900 - 10.1109/LMWT.2026.3676313https://www.scopus.com/pages/publications/105035187836
Rights	© 2026, the Authors. This work is licensed under a Creative Commons Attribution 4.0 License. For more information, see https://creativecommons.org/licenses/by/4.0 - https://creativecommons.org/licenses/by/4.0/
Download date	2026-11-02 01:19:04
Item downloaded from	https://hdl.handle.net/10468/19045

UCC
University College Cork, Ireland
Coláiste na hOllscoile Corcaigh

This article has been accepted for inclusion in a future issue of this journal. Content is final as presented, with the exception of pagination.

Co-Designed Quasi-Reflectionless Low-Noise Amplifier With Bandpass Filter and RF Switching Functionalities

Steven Matthew Cheng, *Graduate Student Member, IEEE*, Andrés Fontana, *Member, IEEE*, and Dimitra Psychogiou, *Senior Member, IEEE*

***Abstract*—In this letter, a reflectionless low-noise amplifier (LNA) filter (RLNAF) is presented, incorporating four distinct functions: 1) filtering; 2) reflection cancellation; 3) low-noise amplification; and 4) RF switching within a single component. It is comprised of a transmissive path and two absorptive paths. Specifically, a complex-termination methodology is applied to the transmissive path incorporating a bandpass filter (BPF) and LNA functionalities, removing the need for additional interstage matching networks (MNs). The absorptive paths are composed of a bandstop filter terminated with a loading resistor in one port to selectively dissipate the out-of-band reflected RF signals. Moreover, switch-off functionality is demonstrated by reconfiguring the bias of the transistor. For proof-of-concept validation purposes, two RLNAF prototypes are designed, manufactured, and measured at C-band. The RF characteristics are given as follows: RLNAF I: f_{cen} = 4.65 GHz, gain = 15.8 dB, noise figure (NF) = 2.07 dB, and quasi-reflectionless characteristics better than 10 dB from DC to 4.27 and 4.34 GHz to 6.42 GHz and at least 9.8 dB from 4.27 to 4.34 GHz; RLNAF II: f_{cen} = 3.7 GHz, gain = 15.3 dB, NF = 1.09 dB, and quasi-reflectionless characteristics better than 10 dB from DC to 4.75 and 5.75 GHz to 7.03 GHz and at least 6 dB from 4.75 to 5.75 GHz.**

***Index Terms*—Absorptive filter, bandpass filter (BPF), bandstop filter, low-noise amplifier (LNA), reflectionless filter.**

I. Introduction

THE continuous advancement of wireless communication systems and the new era of 5G+/6G networks impose stringent requirements in the implementation of modern RF front-ends (RFFEs) requiring compact size, low loss, and the ability to support multiband and multistandard applications. One of the key solutions in addressing size compactness and performance enhancement is the co-design of two of its main components, namely, the bandpass filter (BPF) and the low-noise amplifier (LNA). Then, conventional matching networks (MNs) can be eliminated, reducing the overall size and loss in the RFFE [1], [2], [3], [4], [5], [6], [7], [8], [9].

Several filter amplifiers have been presented in the open technical literature to date, exhibiting compact form factors [2], [3], multiband and multistandard capabilities [4], [5], and reconfigurable modes of operation [6], [7], [8], [9]. Specifically, a filter-integrated LNA with a gain of 22 dB at 29 GHz is shown in [2]. To enable multiband- and diplexer-type operation, a split-type resonator-based filter LNA with gains of 18.3 and 15.9 dB at 2.57 and 3.26 GHz, respectively, was demonstrated in [5]. In terms of reconfigurable filter LNAs, a tunable filtering LNA with a gain between 16.7 and 14.2 dB across a tuning range from 2.8 to 4 GHz was discussed in [7]. Although these architectures facilitate size compactness, multistandard operation, and reconfigurability, the majority of the RFFEs are implemented by cascading in-series filters, MNs, and transistors, leading to a high component count [Fig. 1(a)]. Furthermore, they show reflective characteristics; as such, the out-of-band RF signals are reflected back at the input terminal as shown in Fig. 1(c). These undesired RF signal reflections can lead to adverse consequences on subsequent and preceding active stages, such as frequency conversion and amplifying blocks [10]. Mitigation of RF power reflection is conventionally achieved by inserting an RF isolator between the active element and the reflective-type component. However, these passive- and active-type isolators are bulky or consume extra DC power.

A more efficient method of eliminating unwanted RF signal power reflections has been recently demonstrated through the use of reflectionless BPFs that are designed to dissipate the nontransmitted out-of-band RF signal instead of reflecting it back to the source [11]. Typical examples of this approach include single-band reflectionless BPFs having wideband passband characteristics from 3.1 to 5.3 GHz with reflectionless behavior of 10 dB from 10 MHz to 26 GHz [12]. On the other hand, [13] presented a dual-band reflectionless BPF at 14.52 and 15.2 GHz with an absorption level of 9.7 dB from 12.83 to 17.28 GHz. In [14], reconfigurability is incorporated in the reflectionless BPF, enabling tunable response from 2.68 to 3.4 GHz while having quasi-reflectionless behavior from 2 to 4 GHz. In terms of integrating reflectionless characteristics with amplifiers, [15] showed an amplifier designed with an input absorptive network. It exhibited an input reflectionless level of 10 dB from DC to 60 GHz. However, due to its high-noise figure (NF), an additional high-gain LNA is required as its preceding stage. Moreover, frequency selectivity is not incorporated, leading to the need for additional filtering blocks in the RF chain.

Considering the aforementioned challenges, this work presents a novel reflectionless LNA filter (RLNAF) adding multiple analog RF functionalities, including RF filtering, low-noise amplification, RF switching, and reflection cancellation, as depicted in Fig. 1(b) and (d). The proposed concept is

Received 3 March 2026; accepted 17 March 2026. This work was supported by Research Ireland (RI) under Grant 20/RP/8334. *(Corresponding author: Dimitra Psychogiou.)*

The authors are with the School of Engineering, University College Cork, Cork, T12 K8AF Ireland, and also with the Advanced RF Technology Group, Tyndall National Institute, Cork, T12 R5CP Ireland (e-mail: steven.cheng@tyndall.ie; afontana@ieee.org; dpsychogiou@ucc.ie).

Digital Object Identifier 10.1109/LMWT.2026.3676313

© 2026 The Authors. This work is licensed under a Creative Commons Attribution 4.0 License.
For more information, see https://creativecommons.org/licenses/by/4.0/

This article has been accepted for inclusion in a future issue of this journal. Content is final as presented, with the exception of pagination.

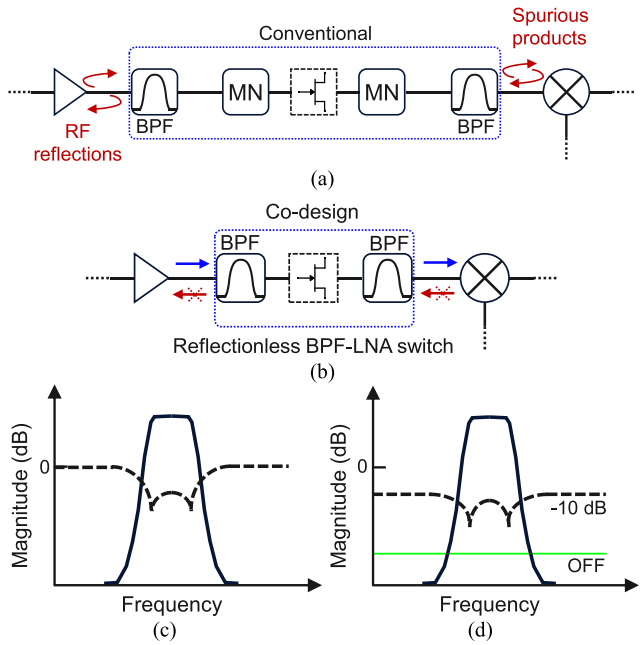


Fig. 1. (a) Conventional RF receiver front-end. (b) Proposed RLNAF with switching functionality comprising two complex-terminated reflectionless RF filters. (c) Synthesized response of (a). (d) Synthesized response of (b).

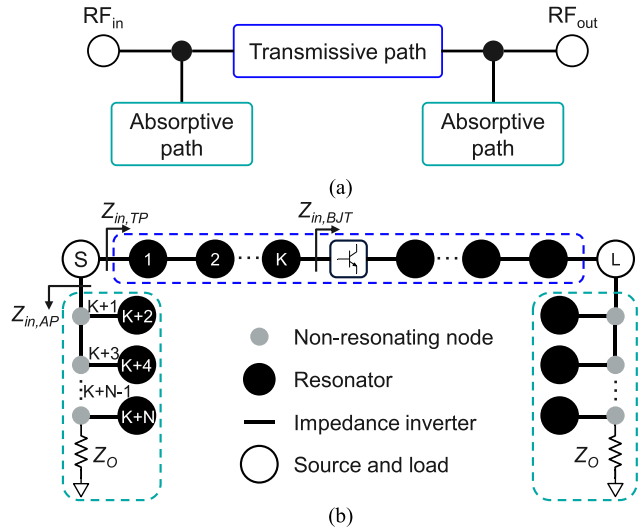


Fig. 2. (a) Conceptual block diagram of the proposed RLNAF concept. (b) Coupling the routing diagram of the proposed RLNAF.

based on a co-designed BPF–LNA transmissive section and a bandstop filtering absorptive section. Owing to the co-design of the RFFE, conventional MNs between stages are eliminated, reducing overall size, complexity, and component count while enabling highly dense multifunctional integration.

II. Theoretical Foundations

The conceptual diagram of the proposed RLNAF is shown in Fig. 2(a). It is based on a complementary diplexer-based concept shaped by a transmissive BPF path and two absorptive BSF paths that have complementary transfer functions. The coupling routing diagram details are shown in Fig. 2(b), wherein the transmissive path is formed by $2K$ in-line resonators that are complex-matched to a bipolar junction transistor (BJT). On the other hand, the absorptive path is a bandstop filtering channel comprised of N resonators and non-resonating nodes with one port terminated by the characteristic impedance $Z_0 = -50\ \Omega$. The transmissive path of the proposed RLNAF determines the in-band characteristics of the entire device by allowing RF signal transmission in its passband range. On the other hand, the BSF-based absorptive paths are connected to their RF input/output and are terminated with a loading resistor on their other end. Thus, the out-of-band RF signal reflected at the input of the transmissive channel is dissipated in the loading resistor of the absorptive channel instead of being reflected back to the source.

A. Design of the Transmissive Path

The design of the transmissive path starts with the BJT, wherein the bias and stability networks are comprised of two independent power supplies fed through RF chokes and stability resistors. The selected bias conditions for this design are $I_b = 17.7\ \mu$A and $V_c = 1.8$ V. In addition, inductive degeneration is applied to improve the tradeoff between gain and noise matching, thus simplifying simultaneous impedance conditions. To directly attach the BPFs to the BJT's input and output, a complex-termination filter design methodology is applied. In particular, only the Kth resonator and inverter are modified to match the impedance of the BJT as discussed in [8]. The complex impedances at the input and output of the BJT are selected for a gain of 15 dB and NF of 0.8 dB from the constant gain and noise circles and are (51 + j14) Ω and (52 + j7.8) Ω.

B. Design of the Absorptive Path

Considering the block diagram of the proposed RLNAF in Fig. 2(b), an input reflectionless behavior can be obtained if its impedances satisfy (1), where $Z_{in,TP}$ and $Z_{in,AP}$ are the normalized input impedance of the transmissive and absorptive paths, respectively. To simplify the analysis, the transistor is approximated as a unilateral device, wherein the output is assumed to have no influence on the input. As such, $Z_{in,TP}$ can be described by (2), where $Z_{in,BJT}$ is the normalized input impedance of the transistor and Y_R is the normalized admittance of the resonating nodes that are synchronously tuned at $\Omega = 0$. Similarly, $Z_{in,AP}$ can be derived using (3) [16]

$$\frac{1}{Z_{in,TP}} + \frac{1}{Z_{in,AP}} = 1 \Longrightarrow |S_{11}| \to \infty \tag{1}$$

$$\frac{1}{Z_{in,TP}} = \frac{M_{s1}^2}{Y_R + \cfrac{M_{12}^2}{Y_R + \cfrac{M_{23}^2}{\cdots + \cfrac{M_{K-1,K}^2}{Y_R + M_{K,BJT}^2 \cdot Z_{in,BJT}}}}} \tag{2}$$

$$\frac{1}{Z_{in,AP}} = \frac{M_{s,K+1}^2}{\cfrac{M_{K+1,K+2}^2}{Y_R} + \cfrac{M_{K+1,K+3}^2}{\cfrac{M_{K+3,K+4}^2}{Y_R} + \cfrac{M_{K+3,K+5}^2}{\cdots + \cfrac{M_{K+N-3,K+N-1}^2}{\cfrac{M_{K+N-1,K+N}^2}{Y_R} + M_{K+N-1,K+N+1}^2}}}}. \tag{3}$$

Utilizing (1)–(3), the set of coupling values can be theoretically calculated and determined as outlined in [16]. To validate the design methodology, synthesized examples for a reflectionless bandpass filtering amplifier with

This article has been accepted for inclusion in a future issue of this journal. Content is final as presented, with the exception of pagination.

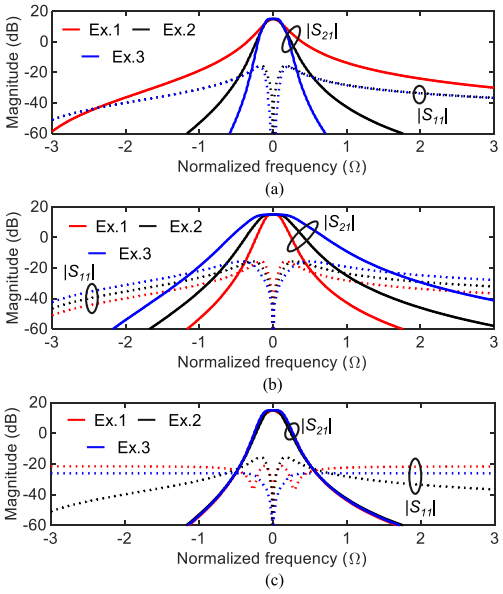


Fig. 3. Synthesized response of the proposed RLNAF shown in Fig. 2(b). (a) S-parameter response for various filter orders. Ex. 1: $M_{S1} = 1.19, K = 1$, and $N = 2$. Ex. 2: $M_{56} = M_{57} = 0.85, K = 2$, and $N = 4$. Ex. 3: $M_{89} = 0.65$, $M_{8,10} = 0.82, K = 2$, and $N = 6$. (b) S-parameter response for various bandwidths. Ex. 1: $M_{56} = 0.85$. Ex. 2: $M_{56} = 1.1$. Ex. 3: $M_{56} = 1.4$. For all examples, $M_{57} = 0.85, K = 2$, and $N = 4$. (c) S-parameter response for unequal filter orders ($K \neq 2N$) for the transmissive and absorptive path. Ex. 1: $N = 2$. Ex. 2: $N = 4$. Ex. 3: $N = 6$. For all examples, $M_{S1} = 1$, $M_{12} = M_{2,BJT} = 1.46, M_{2,2} = -0.39$, and $K = 2$.

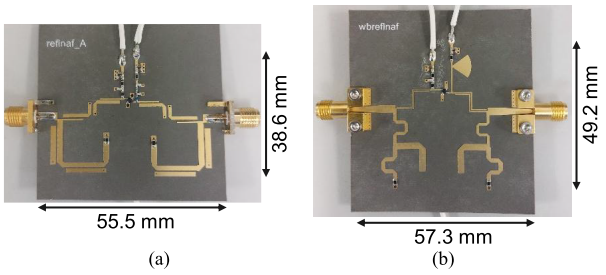


Fig. 4. Manufactured prototypes of the proposed RLNAF concept. (a) RLNAF I. (b) RLNAF II.

$Z_{in,BJT} = 47 + j9$, 7% FBW, and 20-dB passband return loss are shown in Fig. 3. Specifically, transfer function scalability in terms of filter order is shown in Fig. 3(a), while bandwidth reconfigurability is shown for Fig. 3(b). For both synthesized responses, reflectionless input matching is observed across a broad frequency range. Due to the asymmetry arising from the unequal polynomial orders of the transmissive and absorptive paths, full reflection cancellation cannot be achieved, resulting in a quasi-reflectionless response [16], as illustrated by the synthesized response in Fig. 3(c). Nevertheless, the input matching levels remain above 10 dB across a broad frequency range, successfully validating the design equations.

III. Experimental Validation

To validate the proposed RLNAF concept, two prototypes shown in Fig. 4, namely, RLNAFs I and II, were designed, manufactured, and tested. Specifically, RLNAF I is designed for $K = 2$ and $N = 4$ with an FBW of 7%, while RLNAF II is designed for $K = 2$ and $N = 2$ with an FBW of 65%. The co-designed BPF in the transmissive path is implemented

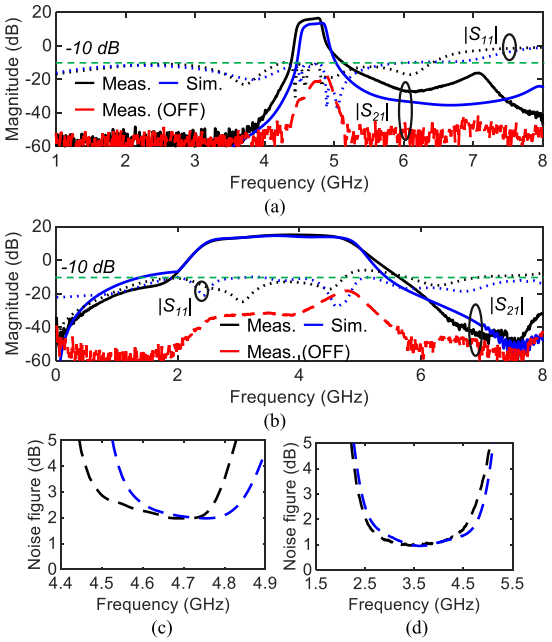


Fig. 5. RF-measured and EM-simulated response of the proposed RLNAFs. (a) S-parameter response of RLNAF I. (b) S-parameter response of RLNAF II. (c) NF of RLNAF I. (d) NF of RLNAF II.

TABLE I
Comparison With State-of-the-Art LNA Filters

	P1	P2	[3]	[4]	[7]
Filtering	Y	Y	Y	Y	N
RF switch	Y	Y	Y	N	N
Reflectionless	Y	Y^{+}	N	N	N
f_{cen} (GHz)	4.65	3.7	4.72	0.11/0.33	3.2
Gain (dB)	15.8	15.3	13.8	16/8.2	15.4
FBW (%)	7.3	57.3	5.1	26/9	1.8
NF (dB)	2.07	1.09	2.26	1.28*	4.0
OIP3 (dBm)	7.0	20.3	14.9	N.A.	25.5
Power (mW)	24	10.5	12.3	20	90
Size (λ_g^2)	1.16	0.94	1.03	0.003	0.75

P1: proposed RLNAF I; P2: proposed RLNAF II; *: simulated; $^{+}$: quasi-reflectionless, *: computed from 1dB compression point.

using microstrip coupled-line resonators and a BJT transistor. In addition, the absorptive path BSF is implemented using coupled-line resonators for RLNAF I and stub-loaded resonators for RLNAF II. The absorptive path implementations in RLNAFs I and II were selected based on manufacturability constraints. Unlike RLNAF I, the required coupling gaps in RLNAF II are smaller than 0.1 mm, making them difficult to implement with conventional CNC-based PCB fabrication. Therefore, stub-loaded resonators are adopted in the RLNAF II absorptive path. The physical parameters of the implemented RLNAFs are derived according to [17] using the coupling coefficients indicated in Fig. 3. All prototypes were manufactured on an RT Duroid 5880 substrate with $\varepsilon_r = 2.2$ and a thickness of 0.8 mm. RF characterization was performed in terms of S-parameters, gain, and NF using a Keysight PNA-X 5244A network analyzer.

The RF-measured characteristics and the EM-simulated response are provided in Fig. 5(a) and (b) for RLNAFs I and II, respectively. The switch-off functionality is achieved by reconfiguring the bias of the transistor ($I_b = 0$ μA), resulting in no power consumption. At the same time, reflectionless

This article has been accepted for inclusion in a future issue of this journal. Content is final as presented, with the exception of pagination.

characteristics are maintained outside the passband owing to the BPF and BSF architecture of the RLNAFs. As observed, the responses are in fair agreement, successfully validating the proposed concept. The discrepancies observed in the manufactured prototype are due to manufacturing tolerances and assembly-induced parasitic effects. The measured RF performance is summarized as follows: 1) RLNAF I: f_{cen} = 4.65 GHz, gain = 15.8 dB, NF = 2.07 dB, OIP3 = 7.0 dBm, reflectionless characteristics of at least 10 dB from DC to 4.27 and 4.34 GHz to 6.42 GHz and at least 9.8 dB from 4.27 to 4.34 GHz, and OFF-state isolation of 24.8 dB; and 2) RLNAF II: f_{cen} = 3.7 GHz, gain = 15.3 dB, NF = 1.09 dB, OIP3 = 20.3 dBm, quasi-reflectionless characteristics of at least 10 dB from DC to 4.75 and 5.75 GHz to 7.03 GHz and at least 6 dB from 4.75 to 5.75 GHz, and OFF-state isolation of 32.3 dB. In addition, the stability factor (μ) was measured to be greater than 1.57 and 1.4 at the operating frequencies of RLNAFs I and II, respectively. The higher NF in RLNAF I as compared to RLNAF II is due to the higher loss in the narrowband filter, which is inherently more lossy than the wideband filter in RLNAF II due to insertion loss being inversely proportional to FBW. To benchmark the proposed RLNAF, Table I compares its performance with state-of-the-art filtering LNAs and reflectionless LNAs most relevant to this work. As observed, the proposed concept facilitates the highest number of functionalities and is the only one that facilitates four functionalities (e.g., filtering, reflection cancellation, low-noise amplification, and switching) within a single RF component while exhibiting comparable gain and NF characteristics. Compared to the reflective LNA filters in [8] and [9], this work implements reflection cancellation, providing enhanced functionality.

IV. Conclusion

In this letter, a co-designed RLNAF is presented for the first time. The proposed concept achieves its reflectionless characteristics by means of two frequency-selective absorption networks alongside a co-designed BPF–LNA. Two prototypes have been validated in the 5G n77 and n79 bands. Specifically, RLNAF I exhibits wide reflectionless characteristics from DC to 6.42 GHz, a gain of 15.8 dB, and an NF of 2.07 dB. RLNAF II shows quasi-reflectionless characteristics from DC to 8.35 GHz, a gain of 15.3 dB, and an NF of 1.09 dB. As demonstrated, the proposed co-design methodology enables miniaturization, component reduction, and facilitates the realization of RFFE chains with minimal reflections, eliminating the need for isolators. This method can be adapted toward quasi-elliptic and diplexing responses, which are to be explored in the future. Moreover, the presented concept can be readily extended toward higher frequencies through the integrated circuits implementation of the resonators and couplings.

References

[1] Y. Gao, X. Shang, L. Li, C. Guo, and Y. Wang, "Integrated filter–amplifiers: A comprehensive review," *IEEE Microw. Mag.*, vol. 23, no. 6, pp. 57–75, Jun. 2022, doi: 10.1109/MMM.2022.3155034.

[2] H.-Y. Li, J.-X. Xu, L. Gao, Q. Xue, and X. Y. Zhang, "24–35 GHz filtering LNA and filtering switch using compact mixed magnetic-electric coupling circuit in 28-nm bulk CMOS," *IEEE Trans. Circuits Syst. I, Reg. Papers*, vol. 70, no. 3, pp. 1071–1082, Mar. 2023, doi: 10.1109/TCSI.2022.3224439.

[3] S. M. Cheng and D. Psychogiou, "Multifunctional single-ended and balanced low-noise amplifiers with co-designed bandpass filtering capabilities," *IEEE Trans. Microw. Theory Techn.*, vol. 73, no. 6, pp. 3334–3343, Jun. 2025, doi: 10.1109/TMTT.2025.3532738.

[4] G. Wibisono, M. Wildan, J. Wahyudi, E. Widoro, and T. Firmansyah, "Co-design structure of dual-band LNA and dual-band BPF for radio navigation aid application," *Wireless Pers. Commun.*, vol. 116, no. 3, pp. 1659–1681, Feb. 2021, doi: 10.1007/s11277-020-07754-9.

[5] S. M. Cheng and D. Psychogiou, "Compact multi-band filter/diplexer LNAs using split-type multi-resonant stages," *IEEE Trans. Circuits Syst. I, Reg. Papers*, vol. 71, no. 10, pp. 4512–4523, Oct. 2024, doi: 10.1109/TCSI.2024.3430376.

[6] M. Al Khoury, B. Jarry, B. Barelaud, and J. Lintignat, "Tunable LNA filter design using coupled-inductor Q-enhancement," *Anal. Integr. Circuits Signal Process.*, vol. 97, no. 2, pp. 323–332, Nov. 2018, doi: 10.1007/s10470-018-1248-8.

[7] M. F. Hagag, M. Abu Khater, and D. Peroulis, "Balanced-balanced tunable filtering LNA using evanescent-mode resonators," in *IEEE MTT-S Int. Microw. Symp. Dig.*, Boston, MA, USA, Jun. 2019, pp. 13–16, doi: 10.1109/MWSYM.2019.8700796.

[8] S. M. Cheng and D. Psychogiou, "Multimode low noise amplifier filter with tunable transfer function characteristics," *IEEE Trans. Microw. Theory Techn.*, vol. 73, no. 3, pp. 1487–1501, Mar. 2025, doi: 10.1109/TMTT.2024.3449135.

[9] A. Fontana, S. Matthew Cheng, and D. Psychogiou, "Reconfigurable and highly-miniaturized low-noise amplifiers based on tunable filtering loads," *IEEE Access*, vol. 13, pp. 51718–51728, 2025, doi: 10.1109/ACCESS.2025.3548311.

[10] R. Gomez-Garcia, D. Psychogiou, J.-M. Munoz-Ferreras, and L. Yang, "Avoiding RF isolators: Reflectionless microwave bandpass filtering components for advanced RF front ends," *IEEE Microw. Mag.*, vol. 21, no. 12, pp. 68–86, Dec. 2020, doi: 10.1109/MMM.2020.3023222.

[11] M. A. Morgan, *Reflectionless Filters*. Norwood, MA, USA: Artech House, 2017.

[12] C. Liu, Z. Deng, X. Liu, and X. Luo, "A wideband bandpass filter with broad stopband and ultra-wide reflectionless range for 5G applications," in *IEEE MTT-S Int. Microw. Symp. Dig.*, Jun. 2019, pp. 834–837, doi: 10.1109/MWSYM.2019.8700856.

[13] M. Malki, L. Yang, and R. Gómez-García, "Ku-band reflectionless single- and dual-band bandpass filters in groove gap waveguide," *IEEE Trans. Microw. Theory Techn.*, vol. 73, no. 9, pp. 5813–5827, Sep. 2025, doi: 10.1109/TMTT.2024.3487633.

[14] K. Zhao, R. Gómez-García, and D. Psychogiou, "Tunable quasi-reflectionless bandpass filters using substrate integrated coaxial resonators," *IEEE Trans. Circuits Syst. II, Exp. Briefs*, vol. 69, no. 2, pp. 379–383, Feb. 2022, doi: 10.1109/TCSII.2021.3094991.

[15] J. D. Ang, L. Yang, R. Gómez-García, and X. Zhu, "A millimeter-wave input-reflectionless amplifier in 45-nm SOI CMOS technology," in *Proc. IEEE Int. Symp. Circuits Syst. (ISCAS)*, May 2024, pp. 1–5, doi: 10.1109/ISCAS58744.2024.10557953.

[16] R. Gómez-Garcia, J.-M. Muñoz-Ferreras, and D. Psychogiou, "High-order input-reflectionless bandpass/bandstop filters and multiplexers," *IEEE Trans. Microw. Theory Techn.*, vol. 67, no. 9, pp. 3683–3695, Sep. 2019, doi: 10.1109/TMTT.2019.2924975.

[17] J.-S. Hong, *Microstrip Filters for RF/Microwave Applications*, 2nd ed., Hoboken, NJ, USA: Wiley, 2011.